



Study of locust bean gum reinforced cyst-chitosan and oxidized dextran based semi-IPN cryogel dressing for hemostatic application



Lalit Kumar Meena ^a, Pavani Raval ^b, Dhaval Kedaria ^a, Rajesh Vasita ^{a,*}

^a School of Life Sciences, Central University of Gujarat, Sector-30, Gandhinagar 382030, India

^b Government Engineering College, Sector-28, Gandhinagar 382028, India

ARTICLE INFO

Article history:

Received 28 July 2017

Received in revised form

15 October 2017

Accepted 21 November 2017

Available online 8 December 2017

Keywords:

Chitosan

Oxidized dextran

Locust bean gum

Cryogel

Hemostasis

ABSTRACT

Severe blood loss due to traumatic injuries remains one of the leading causes of death in emergency settings. Chitosan continues to be the candidate material for hemostatic applications due to its inherent hemostatic properties. However, available chitosan-based dressings have been reported to have an acidic odor at the wound site due to the incorporation of acid based solvents for their fabrication and deformation under compression owing to low mechanical strength limiting its usability. In the present study semi-IPN cryogel was fabricated via Schiff's base cross-linking between the polyaldehyde groups of oxidized dextran and thiolated chitosan in presence of locust bean gum (LBG) known for its hydrophilicity. Polymerization at $-12\text{ }^{\circ}\text{C}$ yielded macroporous semi-IPN cryogels with an average pore size of $124.57 \pm 20.31\text{ }\mu\text{m}$ and 85.46% porosity. The hydrophobicity index of LBG reinforced semi-IPN cryogel was reduced 2.42 times whereas the swelling ratio was increased by 156.08% compare to control cryogel. The increased hydrophilicity and swelling ratio inflated the compressive modulus from 28.1 kPa to 33.85 for LBG reinforced semi-IPN cryogel. The structural stability and constant degradation medium pH were also recorded over a period of 12 weeks. The cryogels demonstrated lower adsorption affinity towards BSA. The cytotoxicity assays (direct, indirect) with 3T3-L1 fibroblast cells confirmed the cytocompatibility of the cryogels. The hemolysis assay showed <5% hemolysis confirming blood compatibility of the fabricated cryogel, while whole blood clotting and platelet adhesion assays confirmed the hemostatic potential of semi-IPN cryogel.

© 2017 The Authors. Production and hosting by Elsevier B.V. on behalf of KeAi Communications Co., Ltd. This is an open access article under the CC BY-NC-ND license (<http://creativecommons.org/licenses/by-nc-nd/4.0/>).

1. Introduction

Hemorrhage due to traumatic injuries and post-operative blood loss remain one of the prime causes of loss of life in emergency and hospital settings [1]. The body's hemostatic mechanisms fail to deliver hemostasis in cases of uncontrollable bleeding caused by damage to major vasculatures. Natural polymers such as chitosan, collagen [2] and oxidized regenerated cellulose [3] have been extensively used in fabricating hemostatic dressings. Chitosan remains the candidate material for devising wound dressings due to its intrinsic properties such as ability to bring upon hemostasis [4], biocompatibility [5], degradability [6], mucoadhesivity [7] and antibacterial properties [8]. Owing to the presence of protonable

amine terminals on the chitosan polymer, they successfully attract negatively charged RBC membranes bringing about aggregation of RBCs and blood components [9]. Moreover, its ability to be devised into hydrogels and other porous scaffolds due to its efficient gel-forming properties make them desirable for biomedical applications [10,11]. Fast swelling chitosan based hydrogels added to the hemostatic property of the chitosan [12,13]. However, increase in the porosity of the hydrogels decreased their mechanical strength. Covalently bonded irreversible chitosan hydrogels which were found to have higher mechanical strength than physically associated chitosan hydrogels [14] could be formed by dialdehyde cross-linkers such as glutaraldehyde and glyoxal. However their high reactivity and toxicity have limited their applications as cross-linkers for biomedical systems [15,16]. Therefore it is desirable to look into *in situ* polymerization techniques.

Dextran a natural polysaccharide, having vicinal hydroxyl groups give seat to sodium periodate based oxidation generating polyaldehyde groups [17] which can readily participate in gelation

* Corresponding author.

E-mail address: rajesh.vasita@gmail.com (R. Vasita).

Peer review under responsibility of KeAi Communications Co., Ltd.

as observed in fabrication of *in situ* hydrogels of N-carboxymethylated chitosan and oxidized dextran [18] and thiolated chitosan and oxidized dextran [19]. The formation of double networks (DNs) or Interpenetrating Polymer Networks (IPNs) are found to be effective means to increase the mechanical strength of the hydrogels [20,21]. The swelling rates, solute diffusion and equilibrium water contents [22–24] of the IPN and semi-IPN type hydrogel were also found to improve along with mechanical strength [25] for hemostasis application [26]. In our study modified cyst-chitosan was used with LBG for cryogel fabrication and its application for hemostasis was demonstrated. Cyst-chitosan has several advantages over chitosan like water solubility which ensures acid-free fabrication of cryogel. Availability of two types of functional groups (amino and thiol groups) improves the cross-linking ability and functionality of polymer for biological applications. LBG improves water absorption by its free hydroxyl groups, mechanical strength via higher molecular weight polymeric chains and elasticity of semi-IPN cryogel. The semi-IPN cryogel have some advantages over commercially available chitosan based hemostatic dressings. The commercially available chitosan based hemostatic dressings (Clo-Sur PAD[®], Scion Cardio-Vascular, USA & Instant Clot Pad, Cosmo Medical Inc., Taiwan) cover the major parts of markets. Despite their commercial success an improvement to overcome the acidic odor at the wound site, deformation under compression and fragility of dressings would be desirable [27]. The acid leached from chitosan dressing could induce inflammatory reactions [28]. The commercially available hemostatic dressings should be biocompatible, fast responsive to aqueous system and resistant to shape deformation. The semi-IPN cryogel which is reported in current study contains some of these above-mentioned properties.

Semi-IPN type scaffold fabricated by cryogelation recognized as cryogels further increased the swelling rates due to interconnected macro-porosity. Hydrophilicity further increased the mechanical strength of semi-IPN cryogel and it can be imparted by incorporation of carboxymethylcellulose [29], hyaluronic acid [30], xanthan gum [31], guar gum [32], locust bean gum [33].

To improve upon the mechanical strength, and fast fluid responsiveness aiding blood clotting, water soluble polysaccharide based semi-IPN cryogel hemostatic dressing was designed in the current study. For *in situ* polymerization, dextran was oxidized to act as a cross-linker, whereas chitosan was modified with cysteine to convert it into a water soluble polymer. Locust bean gum (LBG) has been added to the cryogel for its high water absorbing capacity, water retention and mechanical strength. The semi-IPN cryogel

190–310 kDa and Degree of deacetylation 75–85%), dextran (from *Leuconostoc* ssp., Mr (Relative molecular mass) ~ 70 kDa), L-cysteine, N-(3-Dimethylaminopropyl)-N'-ethylcarbodiimide hydrochloride (EDAC), dialysis tubing cellulose membrane (MWCO ~ 12,000 Da), were purchased from Sigma–Aldrich. 5, 5'-dithio-bis-(2-nitrobenzoic acid) (DTNB), diethylene glycol (DEG) and sodium periodate were purchased from SRL chemicals, India. Mouse embryonic fibroblast 3T3-L1 cells were received from NCCS Pune, India. DMEM and Fetal bovine serum (FBS) were purchased from Gibco, USA.

2.2. Modification of chitosan and dextran

Cysteine-chitosan conjugate was obtained via EDAC reaction. 1% (w/v) chitosan solution was prepared in aqueous 1% (v/v) acetic acid followed by addition of 30 mMoles of cysteine and 1 mMoles of EDAC to initiate the reaction. The reaction mixture was incubated in dark for 3 h followed by its purification using dialysis bag (Mw cut-off ~12000 Da) with 5 mM HCl, 5 mM HCl-1% NaCl and 1 mM HCl for 1st, 2nd and 3rd days respectively. Dialyzed solution was then lyophilized and stored in dark at 4 °C.

A mixture of aqueous solutions of 5 gm dextran in 400 mL and molar equivalent sodium periodate was prepared in 100 mL of deionized water respectively which was kept for stirring in dark at RT for 1 h. Molar equivalent DEG was then added to the reaction mixture and dialyzed (Mw cut-off ~ 12000 Da) against deionized water for 3 days followed by its lyophilization and storage at 4 °C.

2.3. Quantification of the degree of modification

2.3.1. Cysteine content determination

The degree of cysteine conjugation on chitosan was calculated by Ellman's assay. 0.4% w/v of Ellman's reagent was added to 2.5 mL reaction buffer (pH 8) followed by addition of 250 µL of test sample. After 15 min of incubation, the reaction mixture was assayed at 412 nm using a UV-VIS spectrophotometer (Hitachi U-2900). Cysteine was used for standard curve preparation.

2.3.2. Degree of oxidation

The reaction between 0.1 g test sample and hydroxylamine hydrochloride-methyl orange solution for 2 h followed by its titration with 0.1 M NaOH to measure the free HCl determined the degree of oxidation of oxidized dextran (Odex) which was calculated using the following equation:

$$\% \text{ oxidation} = \frac{(\text{Volume in ml}_{\text{NaOH}} \times 10^{-3} \text{ moles} \times M_{\text{NaOH}} \times \text{Molecular weight}_{\text{Dextran monomer}})}{(\text{Weight in gm}_{\text{Odex}})} \times 100 \quad (1)$$

was characterized for morphology, porosity, hydrophilicity, swelling, and mechanical properties. Further the cryogel was studied for degradation behavior and pH change to validate its role for hemostatic dressing. The biocompatibility of the cryogel was determined by cytotoxicity and hemocompatibility studies.

2. Materials and methods

2.1. Materials

Locust bean gum (from *Ceratonia siliqua* seeds, Molecular Weight ~ 310 kDa, M/G = 4:1), chitosan (Molecular weight

2.4. Fabrication of the cryogels

Aqueous solutions of 4% (w/v) cysteine-chitosan and odex were prepared in distilled water. A 2% (w/v) solution of LBG in distilled water was heated at 80 °C for 30 min in a water bath to achieve complete dissolution. Equal volumes of pre-cooled solutions of cysteine-chitosan and LBG were mixed and vortexed for 1 min followed by addition of odex solution in equal volume and the polymeric solution was vortexed again for 1 min to achieve a homogeneous blend. The fabrication mixture was filled in plastic moulds and kept for cross-linking in a pre-chilled methanol-filled cryostat bath (Polystat, Cole-Parmer) at –12 °C for 48 h. After 48 h,

the samples were removed and frozen at $-80\text{ }^{\circ}\text{C}$ overnight. The samples were then lyophilized (FreeZone, Labconco) and stored in air-tight vials at $4\text{ }^{\circ}\text{C}$ until further use.

2.5. Morphological analysis by SEM

Surface morphology of the cryogel was analyzed by scanning electron microscopy (SEM) (EVO 18, Zeiss, Germany). The cryogels having 1 mm thickness were sliced and sputter coated with gold-palladium for 3 min (SC7620 sputter coater, Quorum). The gold coated cryogels were analyzed at a working distance from 10 – 15 mm with an acceleration voltage 5–10 kV. SEM images were examined by ImageJ (ImageJ 1.46r) software taking 50 pores in count to calculate the average pore diameter of the cryogels. To observe the 3T3-L1 fibroblast and blood cells adhesion and morphology the samples were washed with PBS then fixed in 2.0% glutaraldehyde for 1 h further washed thrice with 1X PBS, pH 7.4. The samples were then dehydrated with 30%, 50%, 70%, 80%, 90%, 95% and absolute ethanol for 10 min each. Then samples were lyophilized and metal spraying process was performed prior to SEM examination as mentioned above.

2.6. Chemical analysis by FT-IR

Dextran, chitosan, odex, cysteine grafted chitosan and the cryogels were studied for their modification and cross-linking by attenuated total reflection Fourier transform infrared spectroscopy (Nicolet™ iS™5, iD7 ATR FT-IR, Thermo Scientific™, USA). The samples were scanned from 4000 to 600 cm^{-1} with a resolution of 4 cm^{-1} at room temperature. All samples were analyzed in triplicate manner.

2.7. $^1\text{H-NMR}$ analysis

Oxidation of dextran was qualitatively confirmed by $^1\text{H-NMR}$ analysis. Samples for analysis were prepared by dissolving 5 mg dextran and odex separately in 1 mL of D_2O . The $^1\text{H-NMR}$ spectra were recorded by 500 MHz Fourier-Transform Nuclear Magnetic Resonance Spectrometer (AV III 500 MHz, Bruker, Germany). The number of scans was 16.

2.8. Porosity measurement

The porosity of the cryogels, which is directly correlated to void space present in form of interconnected pores, was measured by n-hexane method [13]. 5 mm thick lyophilized cryogels having dry weight (W_d) were immersed into n-hexane solution for 24 h at room temperature followed by their removal from n-hexane and measurement of their wet weights (W_w) after blotting excess of n-hexane from the surface of samples using a moist filter paper. The percentage porosity was calculated by the following equation:

$$\text{Porosity (\%)} = \frac{(W_w - W_d)}{\rho V} \times 100 \quad (2)$$

where W_w is the wet weight of cryogel after immersion in n-hexane, W_d is the dry weight of cryogel before immersion in n-hexane, ρ is the density of n-hexane, and V is the volume of the cryogel scaffold.

2.9. Hydrophobicity index measurement

Hydrophobicity of the cryogels was expressed as H-index. Pre-weighed (W_d) dry cryogel samples of 5 mm thickness were immersed in distilled water and 70% aqueous isopropanol

separately for 36 h at room temperature. The samples were then removed from both the solvents and their swollen weight (W_s) was measured after removal of excess solvent from the surface of the cryogel using a moist filter paper. The cryogel samples' (y) equilibrium mass swelling ratio in solvent x was calculated by the following equation:

$$\text{Equilibrium mass swelling ratio } q_{x,y} = \left(\frac{W_s}{W_d} \right) \quad (3)$$

While H-index for the cryogel samples (y) was calculated by the following equation:

$$\text{H - index of } y \text{ (H}_y\text{)} = \left(\frac{q_{i70,y}}{q_{dw,y}} \right) \quad (4)$$

2.10. Protein adsorption assay

To assess the protein adsorption capacity of the cryogels, bovine serum albumin was used as a model protein molecule. Cryogel samples ($n = 3$) of 5 mm thickness were equilibrated in 1X PBS (pH 7.4) at $37\text{ }^{\circ}\text{C}$ for 24 h. The samples were then removed, and their swollen weight was measured. Next, all the pre-swelled samples were placed separately in 1 mL 0.05% (w/v) BSA solution (pre-prepared in 1X PBS) for 2 h at $37\text{ }^{\circ}\text{C}$ with mild shaking. Then, all the samples were removed from BSA solution and residual BSA into the solution was measured by BCA assay. The optical density of the BCA solution was measured at 562 nm using microplate reader (Synergy H1 Hybrid Reader, BioTek). The amount of BSA adsorbed was calculated by the following equation:

$$\text{Adsorbed BSA} = \frac{C_i - C_r}{m} \times V \quad (5)$$

where C_i and C_r are the initial and residual concentration of BSA solution respectively, V is the volume of BSA solution and m as the weight of the swollen sample.

2.11. Swelling study

The external fluid responsiveness of the cryogels was tested by using the classical gravimetric method at room temperature. Pre-weighed (W_d) dry samples of 5 mm thickness were submerged in distilled water and removed at predetermined time points. The swollen weight (W_s) of the cryogels was measured post removal of excess water from the surface of the cryogels using a moist filter paper. Samples were studied in triplicate and the percentage water uptake was calculated by the following equation:

$$\text{Swelling Ratio (\%)} = \frac{\text{Swollen weight (} W_s \text{)} - \text{Dry Weight (} W_d \text{)}}{\text{Dry Weight (} W_d \text{)}} \times 100 \quad (6)$$

2.12. Mechanical strength analysis

The analysis of mechanical strength of the cryogel samples were performed on a universal testing machine (H5KT, Tinius Olsen). Cylindrical shaped samples having ~ 5.45 mm thickness and ~ 8.36 mm diameter were equilibrated in 1X PBS, pH 7.4 for 6 h prior

to the analysis. All equilibrated samples were subjected to generic compression to evaluate compressive modulus by using a 50 N load cell with a strain rate of 5 mm/min. Horizon software was used to plot the raw data into a stress-strain curve ($n = 3$).

2.13. *In vitro* degradation study

To assess the biodegradability and microstructural stability of the cryogels, *in vitro* degradation study was performed. Pre-weighed (W_0) samples with 12 mm height and ~8.36 mm diameter were sterilized by 70% ethanol for 1 h and freeze dried. The freeze dried samples were then immersed into 30 mL, 1X sterile PBS (pH 7.4) and incubated at 37 °C in a shaking water bath at 50 rpm. The samples were removed at predetermined time points, washed, and freeze dried. The dry weight (W_t) of freeze dried samples and pH of the degradation medium was measured. The percentage degradation was calculated by the following equation:

$$\text{Degradation (\%)} = \frac{W_0 - W_t}{W_0} \times 100 \quad (7)$$

where, W_0 and W_t are the weights of the samples before test and at various time points respectively.

2.14. *In vitro* cytotoxicity assay

Biocompatibility of any device is a primary requirement to confirm its feasibility for biological applications. In this study, the cytotoxicity assays were performed by three different test procedures suggested by ISO 10993-5, 2009 for medical devices. These three test procedures were as follows: test one by indirect contact, where the cryogel discs were incubated with cells monolayer. The second test on leached medium where cryogel discs' leached culture medium was used for cells monolayer culture. The third test was direct contact test, where cells were grown on the cryogel discs. For *in vitro* cytotoxicity assay, 3T3-L1 mouse embryonic fibroblast cells were maintained and cultured in DMEM high glucose medium with 10% FBS at 37 °C with 5% CO₂. Cryogels were sliced in 1 mm thick discs and treated with 1% w/v NaBH₄ for 1 h. The cryogels were sterilized with 70% ethanol for 1 h, followed by UV for 1 h. In 24 well culture plates 1×10^4 cells/well were seeded into two groups. After 24 h of seeding in one group sterilized cryogel discs were placed, while in another group culture medium was replaced with cryogel leached culture medium. After that, alamar blue assay was performed at 24 and 48 for both groups. While for direct contact test 0.42×10^4 cells/cryogel were seeded and incubated for 24 h. Alamar blue assay was performed at 24 and 48 h. After 48 h of culture, some samples were also used for live/dead assay. Cryogel samples were removed from the medium and stained with calcein AM (2 μM) and ethidium homodimer-1 (4 μM) and incubated for 30 min. Then imaging was done with confocal microscope (LSM780, Zeiss, Germany). Cells monolayer on TCPS with complete medium was used as a control and all groups taken as $n = 4$.

2.15. Blood compatibility studies

The studies were approved by the ethical committee of Central University of Gujarat, India. Human blood was drawn from healthy volunteers using a citrated 3 mL sterile B.D. Vacutainer[®] having the ratio of whole blood to anticoagulant as 9:1. All the cryogel samples were used in triplicate ($n = 3$) throughout the studies.

2.15.1. Hemolysis assay

The hemolytic property of the cryogels was assessed by a

hemolysis assay as described elsewhere [34]. Cryogel discs of 3 mm thickness and ~8.36 mm diameter were equilibrated in 0.9% (w/v) NaCl prior to study at 37 °C for 24 h. 0.25 mL of prepared blood was added to the samples followed by addition of 0.9% (w/v) NaCl after 20 min to stop hemolysis. Subsequently, the samples were incubated for 1 h at 37 °C followed by centrifugation at $600 \times g$ (Nuvision Centri- TD4N, Nucleus Inc.) for 45 min. The resulting supernatant was collected and its absorbance was recorded at 540 nm using a spectrophotometer (Spectrophotometer 106, Systronics). 2 mL of distilled water added to 0.25 mL of prepared blood and 0.9% (w/v) NaCl served as positive and negative control respectively. The percentage hemolysis was obtained using the following expression:

$$\text{Hemolysis (\%)} = \left(\frac{OD_{test} - OD_{negative}}{OD_{positive} - OD_{negative}} \right) \times 100 \quad (8)$$

where, OD_{test} is the optical density of the test sample and $OD_{negative}$ and $OD_{positive}$ stand for optical densities of negative and positive controls respectively.

2.16. Whole blood clotting assay

The study was undertaken to demonstrate the blood clotting efficiency of the prepared cryogels. The study was adapted from Ref. [35]. The dry samples were warmed in polypropylene lab ware at 37 °C for 90 min prior to the beginning of the experiments. 0.2 mL of whole blood was added to the cryogels followed by addition of 20 μL 0.2 M CaCl₂ to initiate the clotting process. The samples were next incubated for 10 min at 37 °C. Subsequently, the red blood cells (RBCs) not trapped in the clot were hemolyzed by addition of 25 mL of distilled water without disturbing the clot. The 15 mL volume of distilled water from the above was taken and centrifuged (Laboratory centrifuge R-8C, Remi) at $180 \times g$ for one min. The supernatant was collected and incubated for 1 h at 37 °C and was later recorded for hemoglobin content at 540 nm using a spectrophotometer (Spectrophotometer 106, Systronics). The blood clotting index (BCI) of the semi-IPN cryogels was also calculated using the following expression:

$$\text{Blood Clotting Index (BCI)} = \left(\frac{OD_{test}}{OD_{negative}} \right) \times 100 \quad (9)$$

where, OD_{test} is the absorbance of the sample and $OD_{negative}$ the absorbance of the negative control. The samples used for the blood clotting studies were preserved and utilized for cell morphological examination using SEM as described in section 2.5.

2.17. Platelet adhesion study

The aim of the study was to demonstrate the platelet adhesion ability of the cryogels. The study was adapted from Ref. [36]. Cryogel discs of ~1 mm thickness and ~8.36 mm diameter were used. The blood obtained from donors was centrifuged (Laboratory centrifuge R-8C, Remi) at $180 \times g$ for 20 min to derive platelet rich plasma (PRP). The PRP obtained from multiple donors was pooled to obtain a final volume of 5 mL of PRP. 0.35 mL of prepared PRP was added to dry pre-warmed samples followed by incubation at 37 °C for 1 h. 100 μL of PRP not adhered to the scaffolds was collected and tested for platelet count using an automated hemocytometer (XT-1800i, Sysmex, Japan). 0.35 mL of PRP not in contact with the scaffolds was used as negative control. All the samples were further preserved and processed for SEM analysis as mentioned in section 2.5.

2.18. Statistical analysis

All statistical analysis was performed by GraphPad Prism 5 software. All experimental data obtained was statistically analyzed in triplicate manner unless otherwise mentioned. The statistically significant differences between two groups were determined with $P < 0.05$ by Student t-test. All quantitative data is expressed as mean \pm standard error mean.

3. Results & discussion

3.1. Modifications of chitosan

In order to increase the solubility of chitosan, modification with cysteine amino acid through the EDAC reaction was performed shown in Fig. 1A. Qualitatively cysteine conjugation was confirmed by FT-IR analysis. Fig. 2A shows FT-IR spectrum of native chitosan, which exhibits its characteristic absorbance peaks between the range of 3356 to 3290 cm^{-1} for O-H and N-H stretching vibrations. Absorbance peak at 2868 cm^{-1} is assigned to C-H (asymmetric) stretching vibration. Absorbance peaks obtained at 1653 cm^{-1} and 1558 cm^{-1} were due to carbonyl (C=O) stretching of amide I and amine vibration of chitosan respectively. Cysteine conjugated chitosan FT-IR spectrum exhibited a very weak absorbance peak at 2546 cm^{-1} which are assigned for S-H stretching vibration and an absorbance peak at 1250 cm^{-1} attributed to C-SH bond vibrations. These two characteristic absorbance peaks confirmed the cysteine conjugation on a primary amino group of chitosan backbone. The lower field shift of absorbance peak from 1558 to 1518 cm^{-1} in modified chitosan confirmed the amide bond formation between the amine group of chitosan and carboxylic group of cysteine amino acid [37,38]. Ellman's reagent was used to quantify the conjugated cysteine molecules via sulfhydryl groups. In the reaction, DTNB was used, which reacts with free sulfhydryl groups and produces a mixture of 2-nitro-5-thiobenzoic acid and disulphide. Cysteine conjugation was found to be around 6 $\mu\text{M}/\text{gm}$ of chitosan, which is lower than the cytotoxic concentration ($>100 \mu\text{M}$) of cysteine [39]. The interaction of sulfhydryl and amine groups of conjugated cysteine with water molecules through hydrogen bonding increases the water solubility of chitosan.

3.2. Dextran oxidation

Dextran was oxidized by sodium periodate reaction to devise an alternative to glutaraldehyde based cross-linking. Sodium periodate attacks vicinal hydroxyl groups of anhydroglucose unit and generates two aldehyde groups as shown in Fig. 1B. Primarily, the oxidation of dextran was confirmed qualitatively by FTIR and $^1\text{H-NMR}$ analysis. Fig. 2B shows FTIR spectrum of native dextran and it displays broad absorbance peak at 3330 cm^{-1} , which corresponds to OH stretching. The generation of aldehyde groups on oxidized dextran was confirmed by the presence of absorbance peak at 1732 cm^{-1} which corresponds to C=O stretching of an aldehyde group, while this peak was completely absent on the native dextran spectrum [40].

$^1\text{H-NMR}$ analysis was also performed to confirm the oxidation of dextran. The $^1\text{H-NMR}$ analysis of dextran and oxidized dextran revealed the success of oxidation process to generate aldehyde groups. The $^1\text{H-NMR}$ spectrum of dextran showed (Fig. 2C) a singlet at 4.85 ppm which was assigned to anomeric proton (H1) of α -1,6 linkage between glucopyranose ring, while a weak resonant at 5.20 ppm was assigned for anomeric proton (H1') of α -1,3 linkage. The multiplet peaks from 3.28 to 3.87 ppm were assigned for various protons positions C2, C3, C4, C5, and C6 in the glucopyranose ring [41,42]. The $^1\text{H-NMR}$ solvent peak for dextran and

oxidized dextran spectra was at 4.71 ppm which assigned to deuterium oxide (D_2O). The $^1\text{H-NMR}$ spectrum for oxidized dextran revealed a weak resonant at 9.12 and 8.31 ppm which were assigned to aldehyde protons and absence of these peaks on dextran spectrum confirmed the oxidation of dextran. The low intensity of aldehyde (-CHO) protons indicates a few free aldehyde groups, which may be due to the formation of hemiacetals. The hemiacetal structure was formed by intramolecular transfer of hydrogen atom from vicinal hydroxyl groups to the aldehyde group. The formation of hemiacetal structure was confirmed by the appearance of new peaks in the range of 4.01–5.83 ppm which were assigned to the protons from the hemiacetal structures [43,44]. This qualitative analysis confirmed the successful oxidation of dextran and further the extent of oxidation was quantified by hydroxylamine hydrochloride reaction with aldehyde groups.

The degree of oxidation of dextran was quantified by reaction between hydroxylamine hydrochloride and aldehyde groups. The free hydrochloric acid was quantified by titration with sodium hydroxide and methyl red. The oxidation degree of dextran with an equimolar ratio of sodium periodates and dextran was 52.54%. However, it was approximately half of the theoretical oxidation, because of the formation of hemiacetals. The obtained oxidation degree of dextran was considered to be optimum for polymerization with cysteine modified chitosan.

3.3. Fabrication of the cryogels

To create interconnected porosity in the cryogels, ice crystal formation should be faster than cross-linking between odex and cyst-chitosan. Therefore in the current study, the fabrication mixture was frozen below sub-zero temperature (Fig. 1E) to create a two phase system with a frozen solvent phase where ice crystal formation propagates and acts as porogen to create interconnected porosity and a non-frozen micro-phase with increased polymer and cross-linker concentration resulting in thick channel wall formation within the cryogel. The cross-linking reaction below sub-zero temperature took 48 h to complete. This longer reaction time was optimum to enhance the possibility of maximum involvement of cyst-chitosan amine groups and aldehyde groups of odex in cross-linking. Two types of cryogels were fabricated i.e. semi-IPN cryogel which contained LBG (Fig. 1C and D) and control cryogel which did not contain LBG.

The SEM imaging of lyophilized cryogel showed uniform distribution of pores throughout. The average pore diameter for semi-IPN cryogel and control cryogel was found to be $124.57 \pm 20.31 \mu\text{m}$ and $111.79 \pm 26.01 \mu\text{m}$ respectively (Fig. 3A and C). The pore size distribution of semi-IPN cryogel (Fig. 3B and D) shows 92% pores in the range of 80–160 μm indicating homogeneous porosity, while control cryogel showed 84% pores in the range of 80–160 μm . The increased pore size in the case of semi-IPN cryogel might be due to lower cross-linking density between cyst-chitosan and odex due to the presence of LBG, which is desirable to create larger pores. Most of pores were irregular in shape and thick-walled. The interconnectivity among pores can be witness in longitudinal section of these cryogel (data not shown). Further, the presence of smaller diameter pores within larger diameter pores indicate interconnected porosity. The interconnected pores will help in capillary movement of biological fluid, while their thick walls will help in expansion of the pores during swelling.

The interconnected channels would be desirable for quick absorption of water from the blood leading to entrapment of the RBCs for the formation of blood clot. These features may increase the role of cryogel dressing for hemostatic applications. The chemical interactions among polymeric chains were further confirmed by FT-IR analysis. The covalent cross-linking between aldehyde groups

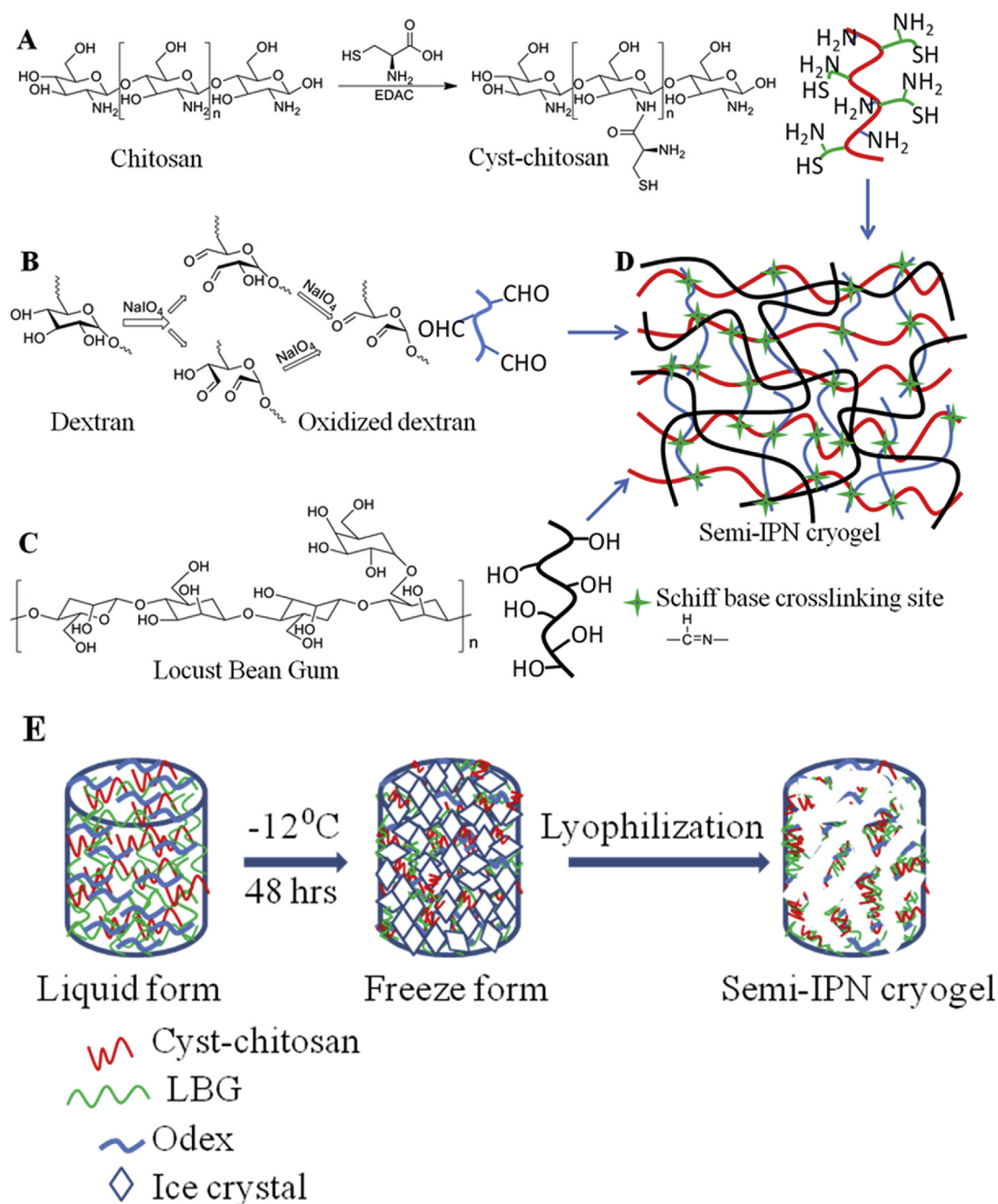


Fig. 1. Schematic illustration of (A) chitosan modification with cysteine; (B) oxidation of dextran; (C) chemical structure of locust bean gum; (D) semi-IPN network and (E) cryogel fabrication scheme.

of odex and amine groups of cyst-chitosan was confirmed by Schiff base interactions. Fig. 3E shows FT-IR spectra where the absorbance peak at 1638 cm^{-1} assigned to stretching vibration of imine bond (C=N) in cryogel is present. In case of semi-IPN no significant peaks shift was observed as compare to control cryogel and hence eliminating the possibilities of any covalent bonding between LBG-cyst-chitosan and LBG-odex. Slightly reduction and broadening of the band at 3306 cm^{-1} can be anticipated due to inter and intrapolymeric hydrogen bonding, which confirms physical entanglement of the LBG polymeric chain. This semi-IPN arrangement of polymeric chains was anticipated for increase in hydrophilicity and mechanical strength of cryogels.

Cryogel's porosity was assessed by a non-polar solvent n-hexane. The n-hexane filled porous channels of the cryogels contributed to the estimation of void space in cryogel, in terms of percentage porosity. The percentage porosity of semi-IPN cryogel was 85.46% whereas 83.80% porosity was obtained for control cryogel. Even after higher values of percentage porosity for both the types of samples, the cryogels were found to be mechanically tougher with their Young's moduli $>28 \text{ kPa}$.

3.4. Hydrophobicity index

The hydrophobicity of the cryogels was assessed using H-index

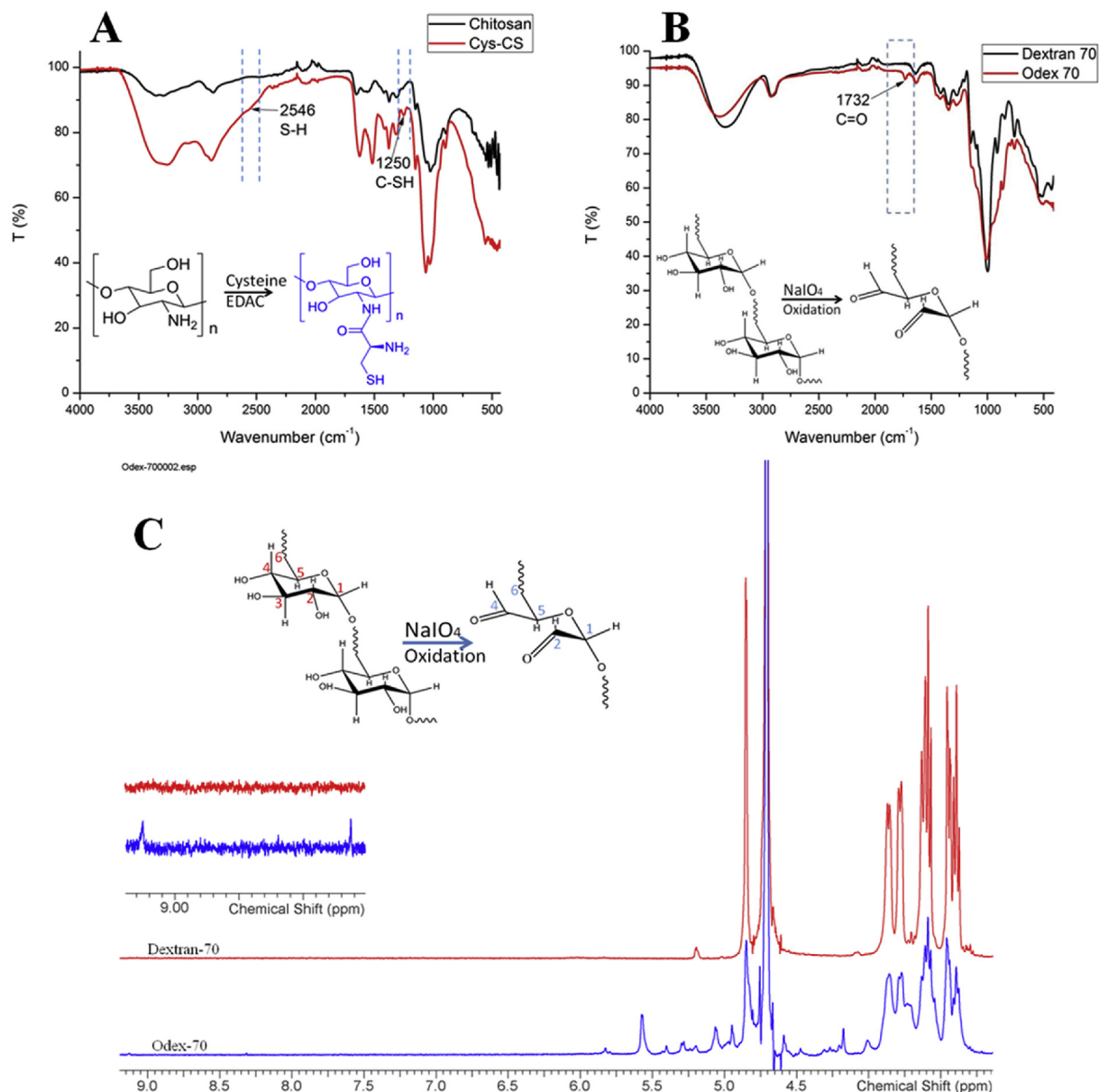


Fig. 2. FT-IR spectra of (A) chitosan powder (Black) and cysteine modified chitosan (Red); (B) dextran powder (Black) and polyaldehyde oxidized dextran (Red); (C) ¹H-NMR spectra of pure dextran-70 powder (Red) and polyaldehyde oxidized dextran (Blue).

as the measured parameter. The presence of hydroxyl group on the backbone of LBG would be important to impart water-loving nature to semi-IPN cryogels. The results showed an H-index of 0.3030 for semi-IPN cryogel while for control cryogel it was 0.7324. The significant reduction in hydrophobicity upon addition of LBG is desirable for efficient swelling and faster fluid absorption rates, which is supported by the data obtained for swelling behavior in section 3.6. The reduction in hydrophobicity will also influence its mechanical property and interaction with biological molecules.

3.5. Protein adsorption on the cryogels

The protein adsorption on the cryogels was assessed by BSA adsorption. To enhance the polymer surface contact with BSA and minimize the BSA entrapment inside the pores, PBS saturated cryogels were used. The amount of BSA adsorption on semi-IPN cryogel was 0.20 ± 0.05 $\mu\text{g}/\text{mg}$ while on control cryogel, it was

0.15 ± 0.08 $\mu\text{g}/\text{mg}$. The amount of protein adsorbed on both samples is not significantly very high. Furthermore there is no significant difference observed between BSA adsorption on semi-IPN and control cryogel. The small amount of albumin adsorption on cryogels may enhance the chances of adsorption of other hemostasis related proteins.

The initial contact of any biomedical device with blood leads to the plasma protein adsorption on the surface of the device. This step will further initiate the adhesion of red blood cells, platelets, and white blood cells [45]. Since the albumin protein adsorption on biomedical device surfaces could inhibit platelet adhesion, and inhibition of blood clot formation [46,47], low albumin adsorption on the cryogels was desirable to have hemostatic potential.

3.6. Swelling study of the cryogels

The liquid absorption capacity of cryogels is one of the major

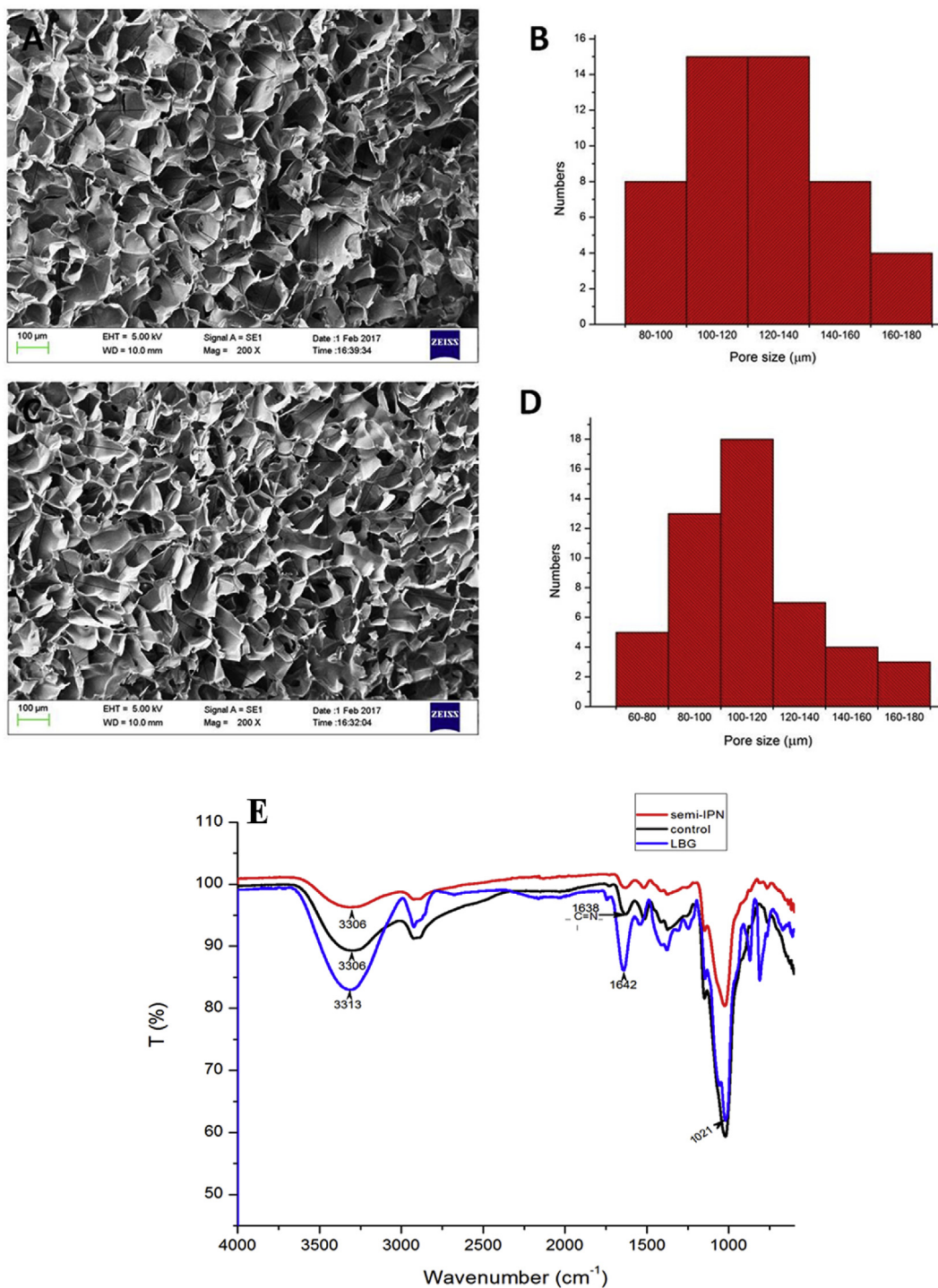


Fig. 3. (A, B) SEM micrographs and pore size distribution histograms of semi-IPN and (C, D) control cryogel (Scale bar 100 μm); (E) FTIR spectra of LBG powder (Blue), semi-IPN (Red) and control cryogel (Black).

factors contributing to the hemostatic property of the material. The swelling study of the cryogels was conducted by gravimetric method at room temperature using distilled water as a solvent. Fig. 4A and B shows the results of the study which reveals that the semi-IPN cryogel reached 99.24% and control cryogel, 99.59% of its equilibrium water content in 1 min respectively indicating a fast absorption rate which can be attributed to the large pore sizes of the cryogels in the macro-porous range and convective flow of the

solvent through the interconnected pores. The average rate of change in the swelling ratio was found to be 92.95 min⁻¹ and 15.76 per min⁻¹ for the first five minutes for semi-IPN and control cryogel respectively. Also, the swelling ratio of semi-IPN cryogel was 2.56 times higher than the control cryogel at equilibrium. The semi-IPN cryogel could absorb water 57 times its own weight at equilibrium, whereas the control absorbed water only 22.87 times its own weight at equilibrium. The higher water holding capacity exhibited

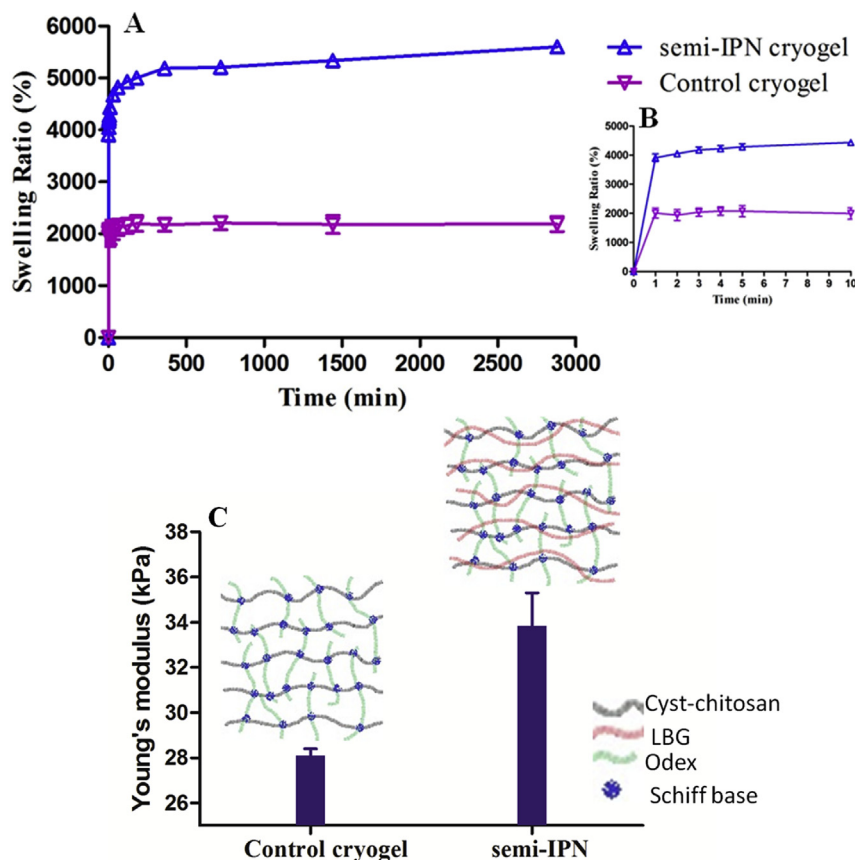


Fig. 4. Swelling study of (A) semi-IPN and control cryogel; (B) inset shows initial fast swelling; (C) Mechanical strength analysis of semi-IPN and control cryogel.

by semi-IPN cryogel may be due to low cross-linking density of polymer network and presence of more hydroxyl groups, which can accommodate more water molecules than control cryogel.

A faster and efficient fluid absorption and holding capacity of semi-IPN cryogel may aid rapid infiltration of the moisture content and blood components from the blood and help to form a concentrated layer of red blood cells at the cryogel-wound interface for achieving faster hemostasis.

3.7. Mechanical strength analysis

Mechanical analysis was performed to confirm the role of the semi-IPN network in imparting mechanical strength to cryogels. The presence of LBG in cryogel imparted a semi-IPN nature to the polymer network, which was absent in the cryogels devoid of LBG. To mimic the physiological conditions, sterile PBS saturated cryogels were used for mechanical analysis. The results showed (Fig. 4C) that bulk's modulus recorded for semi-IPN cryogel was 33.85 kPa while for the control cryogel, it was 28.1 kPa. As showed in the swelling studies, LBG containing cryogel hold more amount of water which is due to hydrogen bond formation between H₂O and hydroxyl groups of LBG. Since water present in a swollen cryogel remains in three states; First, the free water physically entrapped in a matrix that percolated in the matrix during swelling due to capillary forces and can be easily removed by simple squeezing the material, Second are the bound water molecules, which are hydrogen bonded to hydrophilic groups of polymer chains and cannot be easily removed, unless enough force is applied to break the hydrogen bond and finally we have the semi-bound water as described by Omidian et al. [48]. During the

compression of semi-IPN cryogel, the tightly bound water to hydroxyl groups resists its dissociation and imparts mechanical strength. In control cryogel less amount of bound water was present in comparison to semi-IPN. The mechanical strength indicates the ability of the cryogels to prevent the collapse of the porous structure under compression.

3.8. In vitro degradation and pH alteration study

In vitro degradation study directly demonstrates the integrity of the cryogels and its integration in microenvironment. The degradation study was conducted for 12 weeks in PBS, pH 7.4 as degradation medium. The physical weight loss and change in pH of the degradation medium were recorded at predetermined time points, whereas microstructural analysis was performed at the end of 12th week by SEM. The percent weight loss of both the cryogels plotted against time is shown in Fig. 5A. After 1st week the weight loss for semi-IPN cryogel was $23.95 \pm 6.00\%$ while $17.74 \pm 7.68\%$ was observed for control. The higher weight loss in case of semi-IPN can be attributed to lesser cross-linking density and higher swelling rate (see section 3.6), which can swell polymer network much faster and allow leaching of uncross-linked polymer chains. However on successive days no significant difference in degradation was observed in both the cryogels. The average degradation rate for semi-IPN and control cryogel was 4.70% and 4.41% per week. After 2nd week a weight loss of $35.64 \pm 0.47\%$ and $36.90 \pm 0.34\%$ was observed for semi-IPN and control cryogel respectively. After 3rd week a weight loss of $38.54 \pm 0.42\%$ and $39.19 \pm 0.37\%$ was observed for semi-IPN and control cryogel respectively. After 4th to 11th week the weight loss was $42.68 \pm 0.52\%$ and $40.70 \pm 0.23\%$ to

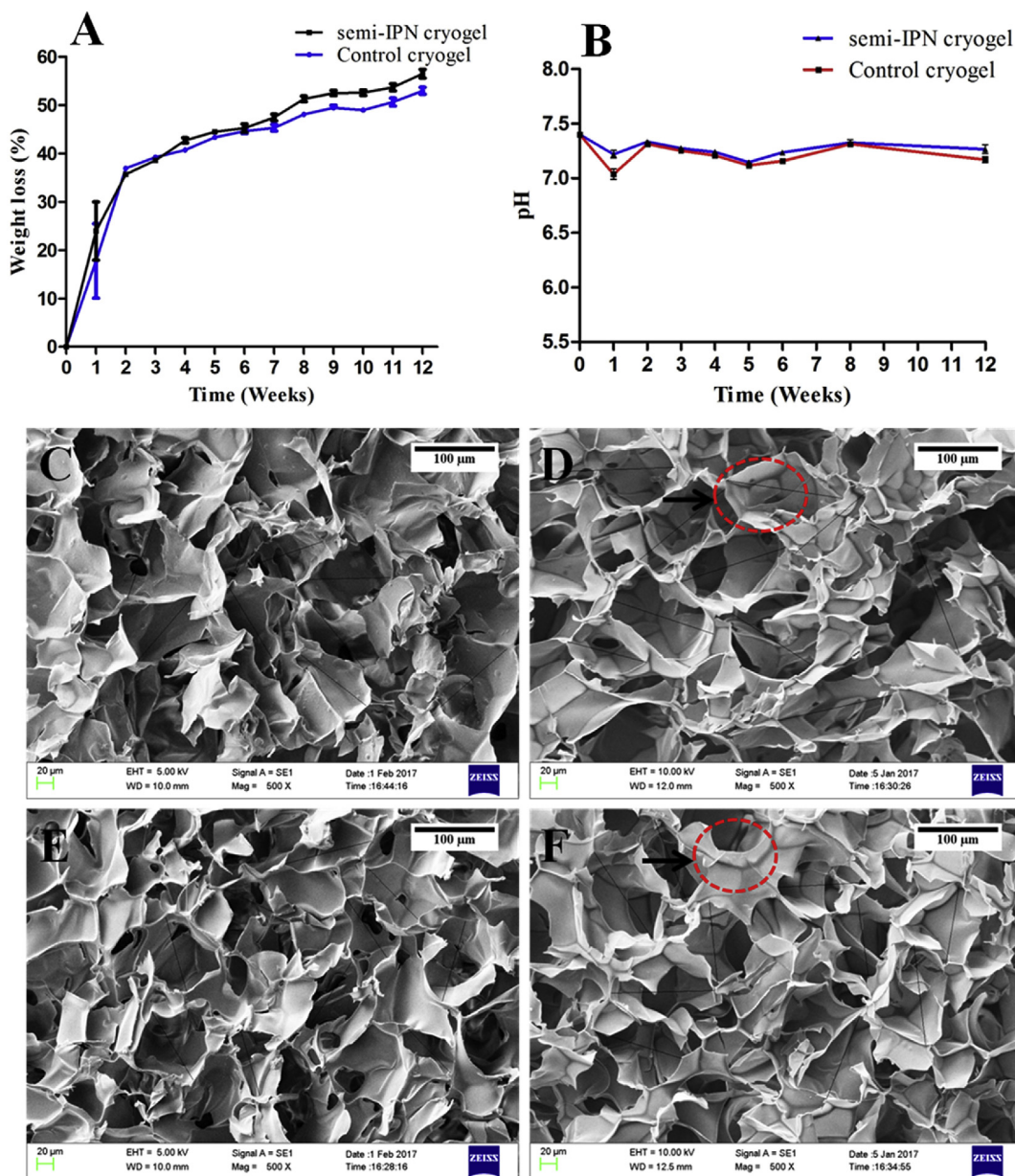


Fig. 5. (A) *In vitro* degradation pattern of semi-IPN and control cryogel ($n = 3$) and (B) pH change of degradation medium during degradation study; (C at 0 days and D at 12th week) SEM micrographs of semi-IPN and (E at 0 days and F at 12th week) control cryogel of degradation.

$53.66 \pm 0.73\%$ and $50.60 \pm 0.81\%$ for semi-IPN and control cryogel respectively. While after 12th week it was $56.47 \pm 0.89\%$ for semi-IPN and $52.94 \pm 0.69\%$ for control cryogel. After 3rd week, the weight loss rate was decreased for both the cryogels and, 15.12% and 11.41% weight losses were observed from 3rd week to 11th week for semi-IPN and control cryogel respectively. A slightly higher weight loss was observed for semi-IPN cryogel. A constant weight loss was observed for both the cryogels which may be due to fast hydrolytic cleavage and pore wall erosion in both cryogels. Further the low cross-linking density in semi-IPN provides a chance to free functional groups to interact with more water molecules. The initial weight loss of cryogels may not affect its internal microstructure (see Fig. 5C–F). The intactness of cryogel microstructure will be helpful in gaseous exchange and fluid flowing during application for hemostasis.

To observe the microstructural changes after degradation study, SEM analysis was performed. SEM micrographs (Fig. 5C–F) of both

types of cryogels after the 12th week of degradation showed pore wall erosion due to polymer degradation. The pore diameter after 12th week of degradation was $130.86 \pm 15.63 \mu\text{m}$ and $112.81 \pm 10.90 \mu\text{m}$ as compare to $124.57 \pm 20.31 \mu\text{m}$ and $111.79 \pm 26.01 \mu\text{m}$ for semi-IPN and control cryogel respectively. The slight increase in pore diameters for semi-IPN cryogels may be due to polymer network relaxation and constant erosion of pore walls. While the low cross-linking density might be another possible reason for increase in pores diameter. Although the almost no change in pore diameter of control cryogel may be due to higher cross-linking density, which resists the polymeric chains relaxations. However the internal microstructure was not distorted by constant degradation and erosion. These results clearly demonstrate that both types of cryogels were very stable during the course of degradation and their microstructure was not compromised after 12th week of degradation. The hydrostatic pressure inside the pore volume and interaction between water and pore

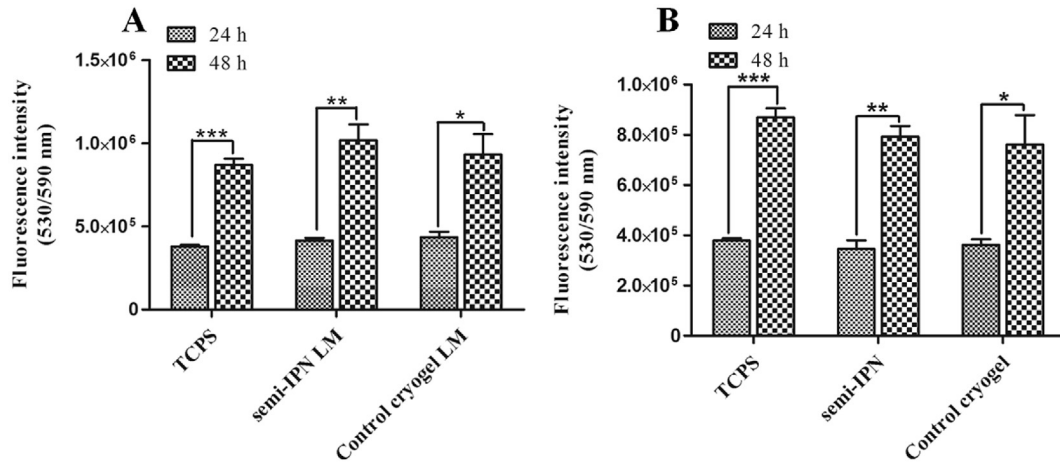


Fig. 6. Cytotoxicity by (A) extract and (B) indirect contact methods through alamar blue assay at 24 and 48 h (*p < 0.05, **p < 0.005, ***p < 0.0005).

will also resist to external compression forces and ensure the structural integrity of cryogel.

The commercially available chitosan-based hemostatic products like Clo-Sur PAD[®], Scion Cardio-Vascular, USA & Instant Clot Pad,

Cosmo Medical Inc., Taiwan, fabrications are acid based [49]. However, in current study not only fabrication but also degradation media was closely recorded for pH change. Results demonstrate (Fig. 5B) that in the case of semi-IPN cryogel the pH fluctuation was

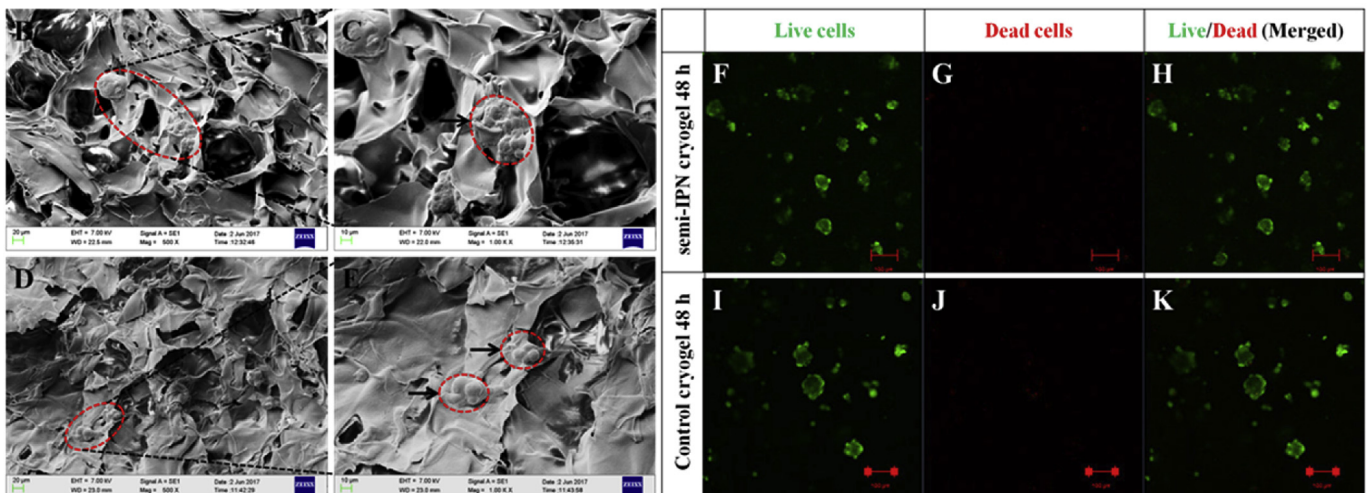
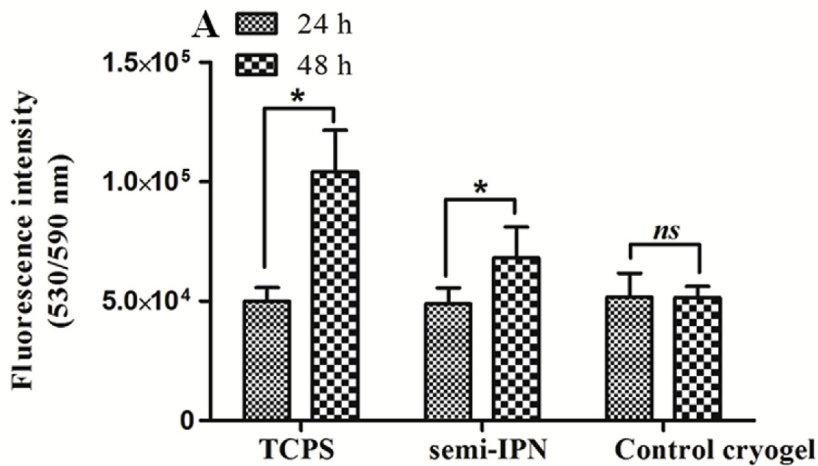


Fig. 7. Cytotoxicity by direct contact method: (A) alamar blue assay at 24 and 48 h; (B, C) SEM micrographs of semi-IPN and (D, E) control cryogel with cultured cells at 48 h; (F–H) Confocal microscope images for semi-IPN and (I–K, S3 supplementary) Control cryogel via Live/dead staining (*p < 0.05).

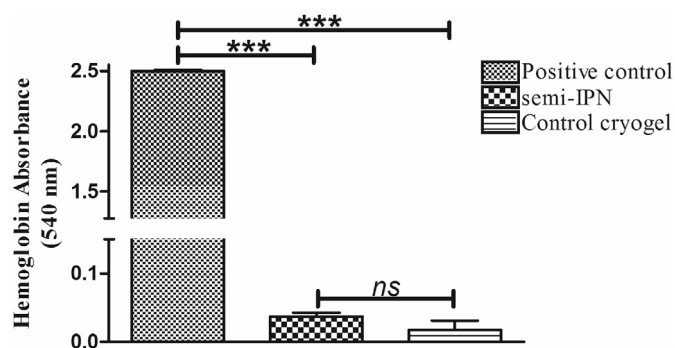


Fig. 8. Blood hemolysis analysis of semi-IPN and control cryogel by *in vitro* hemolysis assay (***) ($p < 0.0001$).

observed from pH 7.4 to pH 7.2 while in the case of control cryogel it was from pH 7.4 to pH 7.1. There was no significant drop in pH of degradation medium observed in both cases. This result ensures the fabrication of acid-free cryogels as potential dressings without acidulous odor. It would be helpful to avoid the allergic reactions, itching, and discomfort at wound site due to acid leaching. The extended intactness of the cryogel without microstructure collapse and maintenance of the physiological pH during degradation shows its merit over commercially available products.

3.9. *In vitro* cytotoxicity assay

The cytotoxicity of cryogels was studied by mouse embryonic fibroblast 3T3-L1 cells viability study. However the base polymers for fabrication of cryogels have been reported biocompatible, but to study any additive toxicity due to the modification of polymers and fabrication process, cytotoxicity assay was performed. The cytotoxicity assay was performed by ISO 10993-5, 2009 guidelines for medical devices. In the case of cryogel incubated in leached medium the cell viability was not significantly compromised for 24 and 48 h as shown in Fig. 6A. The morphology of cells also recorded (see Fig. no S1 in supplementary information) and in all groups slightly elongated cells were observed after 48 h.

In another study, the cryogels were incubated with cells monolayer and cell viability was studied for 24 and 48 h. In this method also no significant changes in cell viability were observed as shown in Fig. 6B. Morphological observations after 48 h showed (see Fig. no S2 in supplementary information) slightly more elongated cells in both semi-IPN and control cryogel compared to TCPS possibly due to a less dense monolayer.

Above showed results indicates that the 3T3-L1 cells with cryogels and leached medium were metabolically active after 48 h, which demonstrates the viability of cells. The morphological analysis by light microscopy further corroborates the alamar blue assay results. In direct contact assay, the 3T3-L1 cells were grown on the cryogels and the metabolic activities were measured. The significant increase in fluorescence intensity was observed from 24 h to 48 h in the case of TCPS and semi-IPN cryogel (Fig. 7A). While for control cryogel the difference in fluorescence intensity between 24 h and 48 h was no significant. The significant increase in fluorescence intensity indicates metabolically active cells proliferation on semi-IPN cryogel. The cell numbers in semi-IPN cryogel was lesser than TCPS surface; however, it is increasing from 24 to 48 h. The slow cell proliferation might be due to the adaptation of cells on scaffold environment at initial time points.

The no significant increase in fluorescence intensity for control cryogel might be due to the adaptation of cells on scaffold environment and dissociation of loosely adhered cells by the time of

medium changing and alamar blue assay performing. While SEM images showed (Fig. 7B–E) spherical morphology of cells which were present in many small clumps attached to the pore wall surface in both the cryogels. The Live/dead assay images (Fig. 7F–K) also showed the cells with green fluorescence in small clumps, which indicates the metabolically live cells presence in a 3-D environment of both cryogel. The absence of red fluorescence indicates absence of dead cells. These results strengthen our observations that the less increase in fluorescence intensity for semi-IPN and no significant increase for control cryogel was not due to cells death. The results of all three tests showed no cytotoxicity of the cryogels to the 3T3-L1 cells after 48 h and validates its *in vitro* cytocompatibility.

3.10. *In vitro* hemolysis assay

Since blood is the first component which comes in contact with the cryogel when applied, this direct contact of the blood with the cryogels could lead to red blood cells destruction [50]. To assess the hemolytic activity of cryogels, *in vitro* hemolysis assay was performed. The results are displayed in Fig. 8, where the absorbance of the samples at 540 nm was recorded. The optical density of the positive control was found to be 2.50 and that of negative control was 0.00. The studies revealed 0.708% hemolysis for control cryogel samples and 1.492% hemolysis for semi-IPN cryogels. The positive control was considered to be 100% hemolytic. The comparison of semi-IPN and control cryogel with the positive control shows negligible hemolysis. The hemolytic potential of the semi-IPN cryogels was found to be slightly higher than control cryogels, however, statistical analysis showed the difference in blood hemolysis to be non-significant. The low blood hemolysis activity of cryogels also corroborates the previously reported results [51,52]. The observation of result validates blood compatibility of the cryogels for hemostatic uses.

3.11. *In vitro* blood clotting assay

The hemostatic potential of newly fabricated cryogels was examined by whole blood clotting assay. In order to evaluate the clotting efficiency of the cryogels, the samples were subjected to recalcified whole blood for 10 min prior to initiating the hemolysis process by adding distilled water to hemolyzed RBCs not trapped in the clot. A higher amount of hemolysis, therefore, indicates lower blood clotting efficiency, clot holding efficiency and a slower clotting time. Fig. 9E showed a 2.25 fold increase in hemolysis was observed for the control cryogel when compared with semi-IPN cryogels. The Blood Clotting Index (BCI) was calculated using equation (9). A lower blood clotting index (BCI) indicates better clotting efficiency of the material. The BCI obtained for semi-IPN cryogel and control cryogel was 1.21 and 3.94 respectively. According to Fig. 9A and B, the results clearly indicate that the whole blood clotting efficiency of semi-IPN cryogel is higher than control cryogel. This significant difference in blood clotting could be due to higher swelling and fast absorption of water from blood by semi-IPN cryogel [53,54]. This leads to the creation of a pool of concentrated blood components consequently aiding the formation of a dense clot. The semi-IPN network increases the chances of lower cross linking density which directly creates more free cationic groups on cyst-chitosan. These free cationic groups might be one of the factors leading to the entrapment of negatively charged RBCs into the blood clot. Further SEM analysis of blood clotted cryogels was also performed to examine the blood clot networks components. Fig. 9A and B revealed a dense fibrin mesh formed with RBCs trapped in it indicating a blood clot formed locally possibly due to ionic interaction between the semi-IPN cryogel surface and

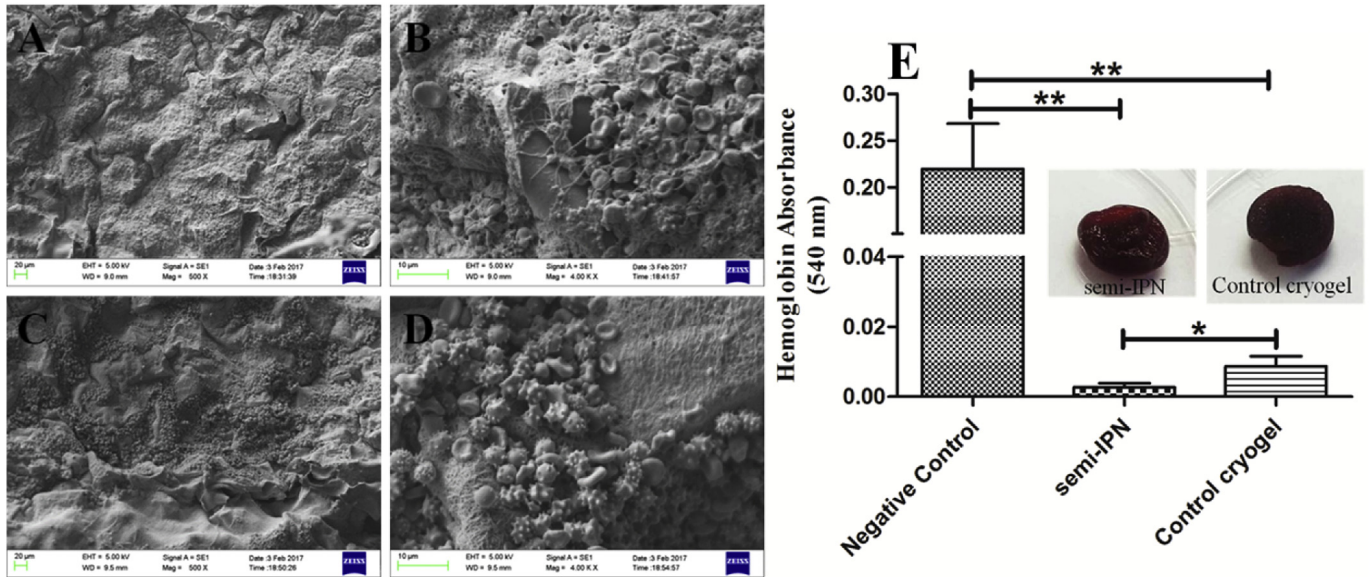


Fig. 9. *In vitro* whole blood clotting: (A, B) SEM micrographs of semi-IPN cryogel; (C, D) Control cryogel clotted blood; (E) Quantitative measurement of blood clotting efficiency via hemoglobin detection (Scale bar A, C 20 and B, D 10 μm) (* $p < 0.05$, ** $p < 0.001$).

entrapped RBCs. Fig. 9C and D shows the deposition of a finer fibrin mesh with fewer RBCs trapped into the mesh because of lesser ionic interactions between the control cryogel surface and the RBCs. The whole blood clotting study confirms the potential of semi-IPN cryogel as a hemostatic dressing.

Since whole blood clotting mainly depends on ionic interactions between the cryogel and RBCs, platelet adhesion and activation also play a major role in hemostasis.

3.12. *In vitro* platelet adhesion study

The platelet adhesion assay was performed to confirm the role of cryogels in platelet adhesion and activation. Semi-IPN cryogel

and control cryogels were in contact with the platelet rich plasma suspensions for 1 h at 37 °C. The number of platelets remaining after contact with the cryogels was compared with the platelet counts in 0.35 mL of PRP, not in contact with any of the scaffolds which served as negative control for the study. The test volume for determining the platelet count was 100 μL throughout the experiment. Fig. 10E shows that the number of platelets adhered to the semi-IPN cryogel and control cryogel did not show any significant difference in cell count. On an average, 29.6×10^3 and 31.6×10^3 platelets adhered to the semi-IPN cryogel and control cryogel respectively. However, the microscopic examination of the samples from the platelet adhesion study under SEM showed (Fig. 10A and B) numerous platelets adhered uniformly to the surface of the

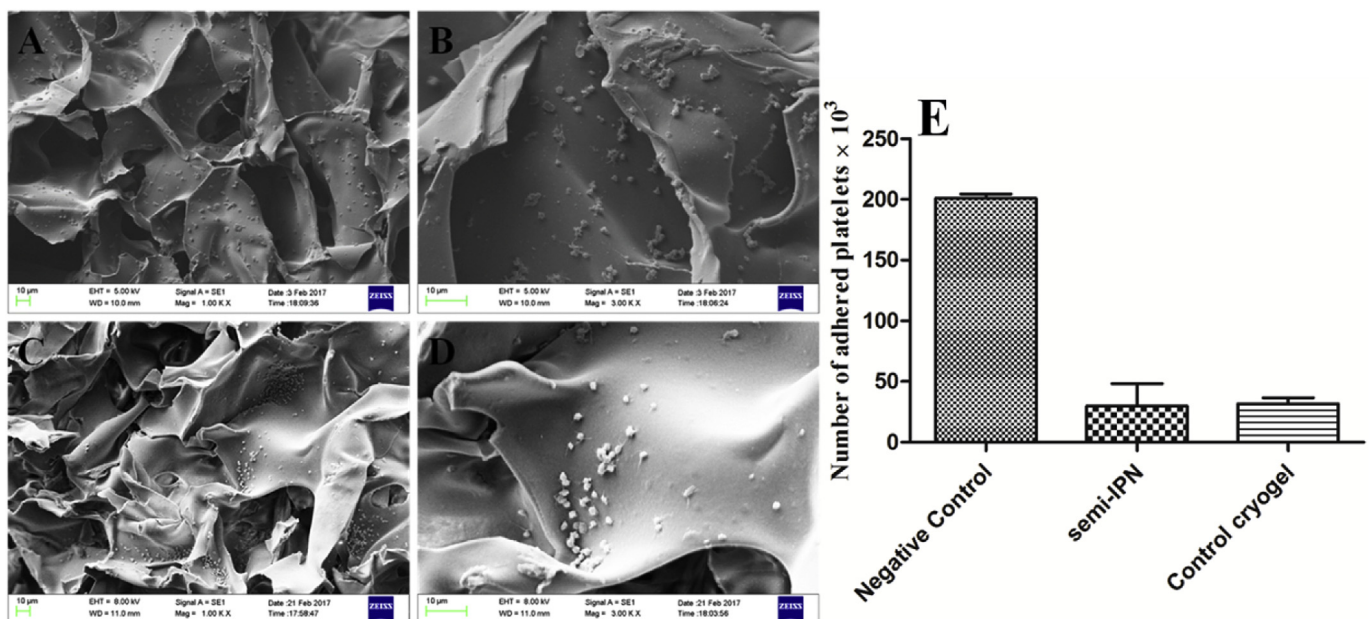


Fig. 10. *In vitro* Platelet adhesion: (A, B) SEM micrographs of semi-IPN cryogel; (C, D) Control cryogel with adhered platelets; (E) Quantitative measurement of adhered platelets on semi-IPN and control cryogel (Scale bar 10 μm).

semi-IPN cryogel with a visible change in platelets morphology. Platelets clusters were also found adhering to the surface with pseudopodia formation and spreading across the pore wall of the semi-IPN cryogel indicating strong adherence to the material. While, the SEM observation (Fig. 10C and D) of control cryogel shows platelets adhesion and activation with pseudopodia but distribution was not uniform. Maximum platelets adhered to low lying areas like blind pores surface. However, platelet adhesion and activation was observed on both types of cryogels. One major achievement of this assay was that without the use of CaCl_2 as a platelet activation factor, platelet activation and pseudopodia formation was observed. This platelet activation might be due to cationic charges of cyst-chitosan and hydrophilic nature. The cryogel materials' integral property, high porosity, swelling capacity and fast water absorption makes the cryogel suitable for platelet adhesion. The platelet adhesion and activation further validates the hemostatic potential of the semi-IPN cryogel.

4. Conclusions

In the present study, fast water absorbing, macro porous, semi-IPN cryogel was prepared for hemostatic applications. To avoid the use of acid based solvent and toxic cross linker in fabrication, chitosan was modified with cysteine amino acid and dextran was partially oxidized. The optimum concentrations of cyst-chitosan, odex, and LBG were optimized for semi-IPN cryogel fabrication. The LBG was used to enhance the hydrophilicity, water absorption capacity and the mechanical strength of semi-IPN cryogel. The semi-IPN cryogel was investigated for its swelling, *in vitro* degradation, pH alteration, and protein adsorption properties. The result shows high swelling ratio, biodegradability in a controlled manner without microstructure collapse, no significant pH alteration and low serum albumin adsorption. These observations validate the semi-IPN cryogels could be used as a hemostatic dressing. Further, the cytotoxicity, blood compatibility, whole blood clot and platelet adhesion studies results proved semi-IPN cryogel as an active hemostatic dressing. Our finding suggests that fabrication of semi-IPN cryogel based on water soluble modified polysaccharides with macro-porosity, high water absorbability, cytocompatibility as well as blood compatibility can be used for hemostatic applications.

Acknowledgments

The author acknowledges the University Grant Commission (Govt of India) for a senior research fellowship. The author would like to thank Unipath Specialty Laboratory Pvt. Ltd. Ahmedabad for their assistance in performing the blood compatibility studies. The RV acknowledges the GSBTM (GSBTM/MD/Projects/SSA/1431/2014-15) for providing the financial support.

Appendix A. Supplementary data

Supplementary data related to this article can be found at <https://doi.org/10.1016/j.bioactmat.2017.11.005>.

References

- [1] A.M. Behrens, M.J. Sikorski, P. Kofinas, Hemostatic strategies for traumatic and surgical bleeding, *J. Biomed. Mater. Res. A* 102 (2014) 4182–4194.
- [2] J.-P. Chen, G.-Y. Chang, J.-K. Chen, Electrospun collagen/chitosan nanofibrous membrane as wound dressing, *Colloids Surf. Physicochem. Eng. Asp.* 313 (2008) 183–188.
- [3] J.H. Voormolen, J. Ringers, G.T. Bots, A. van der Heide, J. Hermans, Hemostatic agents: brain tissue reaction and effectiveness. A comparative animal study using collagen fleece and oxidized cellulose, *Neurosurgery* 20 (1987) 702–709.
- [4] J. Yang, F. Tian, Z. Wang, Q. Wang, Y.J. Zeng, S.Q. Chen, Effect of chitosan molecular weight and deacetylation degree on hemostasis, *J. Biomed. Mater. Res. B Appl. Biomater.* 84 (2008) 131–137.
- [5] P.J. VandeVord, H.W. Matthew, S.P. DeSilva, L. Mayton, B. Wu, P.H. Wooley, Evaluation of the biocompatibility of a chitosan scaffold in mice, *J. Biomed. Mater. Res.* 59 (2002) 585–590.
- [6] K.M. Varum, M.M. Myhr, R.J. Hjerde, O. Smidsrod, In vitro degradation rates of partially N-acetylated chitosans in human serum, *Carbohydr. Res.* 299 (1997) 99–101.
- [7] C.-M. Lehr, J.A. Bouwstra, E.H. Schacht, H.E. Junginger, In vitro evaluation of mucoadhesive properties of chitosan and some other natural polymers, *Int. J. Pharm.* 78 (1992) 43–48.
- [8] N.R. Sudarshan, D.G. Hoover, D. Knorr, Antibacterial action of chitosan, *Food Biotechnol.* 6 (1992) 257–272.
- [9] S.B. Rao, C.P. Sharma, Use of chitosan as a biomaterial: studies on its safety and hemostatic potential, *J. Biomed. Mater. Res.* 34 (1997) 21–28.
- [10] S.V. Madhally, H.W. Matthew, Porous chitosan scaffolds for tissue engineering, *Biomaterials* 20 (1999) 1133–1142.
- [11] H. Nagahama, N. Nwe, R. Jayakumar, S. Koiwa, T. Furuike, H. Tamura, Novel biodegradable chitin membranes for tissue engineering applications, *Carbohydr. Polym.* 73 (2008) 295–302.
- [12] H. Hattori, Y. Amano, Y. Nogami, B. Takase, M. Ishihara, Hemostasis for severe hemorrhage with photocrosslinkable chitosan hydrogel and calcium alginate, *Ann. Biomed. Eng.* 38 (2010) 3724–3732.
- [13] P.T. Kumar, V.K. Lakshmanan, T.V. Anilkumar, C. Ramya, P. Reshmi, A.G. Unnikrishnan, S.V. Nair, R. Jayakumar, Flexible and microporous chitosan hydrogel/nano ZnO composite bandages for wound dressing: in vitro and in vivo evaluation, *ACS Appl. Mater. Interfaces* 4 (2012) 2618–2629.
- [14] N.A. Peppas, *Hydrogels in Medicine and Pharmacy*, CRC Press, Boca Raton (Fla.), 1988.
- [15] H.S. Mansur, E. de S. Costa, A.A.P. Mansur, E.F. Barbosa-Stancioli, Cytocompatibility evaluation in cell-culture systems of chemically crosslinked chitosan/PVA hydrogels, *Mater. Sci. Eng. C* 29 (2009) 1574–1583.
- [16] H.W. Leung, Ecotoxicology of glutaraldehyde: review of environmental fate and effects studies, *Ecotoxicol. Environ. Saf.* 49 (2001) 26–39.
- [17] J. Maia, R.A. Carvalho, J.F.J. Coelho, P.N. Simões, M.H. Gil, Insight on the periodate oxidation of dextran and its structural vicissitudes, *Polymer* 52 (2011) 258–265.
- [18] L. Weng, A. Romanov, J. Rooney, W. Chen, Non-cytotoxic, in situ gelable hydrogels composed of N-carboxyethyl chitosan and oxidized dextran, *Biomaterials* 29 (2008) 3905–3913.
- [19] H. Zhang, A. Qadeer, W. Chen, In situ gelable interpenetrating double network hydrogel formulated from binary components: thiolated chitosan and oxidized dextran, *Biomacromolecules* 12 (2011) 1428–1437.
- [20] K. Yasuda, J. Ping Gong, Y. Katsuyama, A. Nakayama, Y. Tanabe, E. Kondo, M. Ueno, Y. Osada, Biomechanical properties of high-toughness double network hydrogels, *Biomaterials* 26 (2005) 4468–4475.
- [21] D. Myung, D. Waters, M. Wiseman, P.-E. Duhamel, J. Noolandi, C.N. Ta, C.W. Frank, Progress in the development of interpenetrating polymer network hydrogels, *Polym. Adv. Technol.* 19 (2008) 647–657.
- [22] E.S. Dragan, M.M. Lazar, M.V. Dinu, F. Doroftei, Macroporous composite IPN hydrogels based on poly(acrylamide) and chitosan with tuned swelling and sorption of cationic dyes, *Chem. Eng. J.* 204 (2012) 198–209.
- [23] P. Matricardi, C. Di Meo, T. Coviello, W.E. Hennink, F. Alhaique, Interpenetrating Polymer Networks polysaccharide hydrogels for drug delivery and tissue engineering, *Adv. Drug Deliv. Rev.* 65 (2013) 1172–1187.
- [24] R.V. Kulkarni, V. Sreedhar, S. Mutalik, C.M. Setty, B. Sa, Interpenetrating network hydrogel membranes of sodium alginate and poly(vinyl alcohol) for controlled release of prazosin hydrochloride through skin, *Int. J. Biol. Macromol.* 47 (2010) 520–527.
- [25] P.S.K. Murthy, Y.M. Mohan, J. Sreeramulu, K.M. Raju, Semi-IPNs of starch and poly(acrylamide-co-sodium methacrylate): preparation, swelling and diffusion characteristics evaluation, *React. Funct. Polym.* 66 (2006) 1482–1493.
- [26] I.-Y. Kim, M.-K. Yoo, B.-C. Kim, S.-K. Kim, H.-C. Lee, C.-S. Cho, Preparation of semi-interpenetrating polymer networks composed of chitosan and poloxamer, *Int. J. Biol. Macromol.* 38 (2006) 51–58.
- [27] P.-L. Kang, S.J. Chang, I. Manousakas, C.W. Lee, C.-H. Yao, F.-H. Lin, S.M. Kuo, Development and assessment of hemostasis chitosan dressings, *Carbohydr. Polym.* 85 (2011) 565–570.
- [28] H. Xie, L. Lucchesi, J.S. Teach, R. Virmani, Long-term outcomes of a chitosan hemostatic dressing in laparoscopic partial nephrectomy, *J. Biomed. Mater. Res. Part B Appl. Biomater.* 100 (2012) 432–436.
- [29] W. Wang, Q. Wang, A. Wang, pH-responsive carboxymethylcellulose-g-poly(sodium acrylate)/polyvinylpyrrolidone semi-IPN hydrogels with enhanced responsive and swelling properties, *Macromol. Res.* 19 (2011) 57–65.
- [30] S.J. Kim, C.K. Lee, S.I. Kim, Characterization of the water state of hyaluronic acid and poly(vinyl alcohol) interpenetrating polymer networks, *J. Appl. Polym. Sci.* 92 (2004) 1467–1472.
- [31] M. Hamcerencu, J. Desbrieres, A. Khoukh, M. Popa, G. Riess, Thermodynamic investigation of thermoresponsive xanthan-poly (N-isopropylacrylamide) hydrogels, *Polym. Int.* 60 (2011) 1527–1534.
- [32] X. Li, W. Wu, W. Liu, Synthesis and properties of thermo-responsive guar gum/poly(N-isopropylacrylamide) interpenetrating polymer network hydrogels, *Carbohydr. Polym.* 71 (2008) 394–402.
- [33] S. Kaity, J. Isaac, A. Ghosh, Interpenetrating polymer network of locust bean

- gum-poly (vinyl alcohol) for controlled release drug delivery, *Carbohydr. Polym.* 94 (2013) 456–467.
- [34] A. Srivastava, A. Kumar, Thermoresponsive poly(N-vinylcaprolactam) cryogels: synthesis and its biophysical evaluation for tissue engineering applications, *J. Mater. Sci. Mater. Med.* 21 (2010) 2937–2945.
- [35] K. Madhumathi, P.T. Sudheesh Kumar, S. Abhilash, V. Sreeja, H. Tamura, K. Manzoor, S.V. Nair, R. Jayakumar, Development of novel chitin/nanosilver composite scaffolds for wound dressing applications, *J. Mater. Sci. Mater. Med.* 21 (2010) 807–813.
- [36] E. Cenni, G. Ciapetti, S. Stea, A. Corradini, F. Carozzi, Biocompatibility and performance in vitro of a hemostatic gelatin sponge, *J. Biomater. Sci. Polym. Ed.* 11 (2000) 685–699.
- [37] R. Esquivel, J. Juárez, M. Almada, J. Ibarra, M.A. Valdez, Synthesis and characterization of new thiolated chitosan nanoparticles obtained by ionic gelation method, *Int. J. Polym. Sci.* 2015 (2015) 1–18.
- [38] G. Xu, L. Cheng, Q. Zhang, Y. Sun, C. Chen, H. Xu, Y. Chai, M. Lang, In situ thiolated alginate hydrogel: Instant formation and its application in hemostasis, *J. Biomater. Appl.* 31 (2016) 721–729.
- [39] Y. Nishiuchi, M. Sasaki, M. Nakayasu, A. Oikawa, Cytotoxicity of cysteine in culture media, *In Vitro* 12 (1976) 635–638.
- [40] X. Zhao, P. Li, B. Guo, P.X. Ma, Antibacterial and conductive injectable hydrogels based on quaternized chitosan-graft-polyaniline/oxidized dextran for tissue engineering, *Acta Biomater.* 26 (2015) 236–248.
- [41] R.J.H. Stenekes, H. Talsma, W.E. Hennink, Formation of dextran hydrogels by crystallization, *Biomaterials* 22 (2001) 1891–1898.
- [42] S.G. Lévesque, R.M. Lim, M.S. Shoichet, Macroporous interconnected dextran scaffolds of controlled porosity for tissue-engineering applications, *Biomaterials* 26 (2005) 7436–7446.
- [43] D.-A. Wang, S. Varghese, B. Sharma, I. Strehin, S. Fermanian, J. Gorham, D.H. Fairbrother, B. Cascio, J.H. Elisseeff, Multifunctional chondroitin sulphate for cartilage tissue-biomaterial integration, *Nat. Mater.* 6 (2007) 385–392.
- [44] J. Maia, L. Ferreira, R. Carvalho, M.A. Ramos, M.H. Gil, Synthesis and characterization of new injectable and degradable dextran-based hydrogels, *Polymer* 46 (2005) 9604–9614.
- [45] B. Singh, A. Dhiman, Design of Acacia gum–carbopol–cross-linked-polyvinylimidazole hydrogel wound dressings for antibiotic/anesthetic drug delivery, *Ind. Eng. Chem. Res.* 55 (2016) 9176–9188.
- [46] D.L. Coleman, D.E. Gregonis, J.D. Andrade, Blood-materials interactions: the minimum interfacial free energy and the optimum polar/apolar ratio hypotheses, *J. Biomed. Mater. Res.* 16 (1982) 381–398.
- [47] I. Dion, C. Baquey, P. Havlik, J.R. Monties, A new model to test platelet adhesion under dynamic conditions. Application to the evaluation of a titanium nitride coating, *Int. J. Artif. Organs* 16 (1993) 545–550.
- [48] H. Omidian, K. Park, Introduction to hydrogels, in: R.M. Ottenbrite, K. Park, T. Okano (Eds.), *Biomedical Applications of Hydrogels Handbook*, Springer, New York, 2010, pp. 1–16.
- [49] P.-L. Kang, S.J. Chang, I. Manousakas, C.W. Lee, C.-H. Yao, F.-H. Lin, S.M. Kuo, Development and assessment of hemostasis chitosan dressings, *Carbohydr. Polym.* 85 (2011) 565–570.
- [50] S. Dawlee, A. Sugandhi, B. Balakrishnan, D. Labarre, A. Jayakrishnan, Oxidized chondroitin sulfate-cross-linked gelatin matrixes: a new class of hydrogels, *Biomacromolecules* 6 (2005) 2040–2048.
- [51] A.A. Romani, L. Ippolito, F. Riccardi, S. Pipitone, M. Morganti, M.C. Baroni, A.F. Borghetti, R. Bettini, In vitro blood compatibility of novel hydrophilic chitosan films for vessel regeneration and repair, in: R. Pignatello (Ed.), *Advances in Biomaterials Science and Biomedical Applications*, InTech, Rijeka, 2013 pp. Ch. 06.
- [52] D. Archana, J. Dutta, P.K. Dutta, Evaluation of chitosan nano dressing for wound healing: characterization, in vitro and in vivo studies, *Int. J. Biol. Macromol.* 57 (2013) 193–203.
- [53] Y. Chen, Y. Zhang, F. Wang, W. Meng, X. Yang, P. Li, J. Jiang, H. Tan, Y. Zheng, Preparation of porous carboxymethyl chitosan grafted poly (acrylic acid) superabsorbent by solvent precipitation and its application as a hemostatic wound dressing, *Mater. Sci. Eng. C* 63 (2016) 18–29.
- [54] A.M. Behrens, M.J. Sikorski, T. Li, Z.J. Wu, B.P. Griffith, P. Kofinas, Blood-aggregating hydrogel particles for use as a hemostatic agent, *Acta Biomater.* 10 (2014) 701–708.